Smart Structures and Systems, *Vol. 35*, *No. 3* (*2025*) *131-140*
https://doi.org/10.12989/sss.2025.35.3.131

Explicit temperature field reconstruction algorithm for concrete based on finite element method

Zhenyang Zhu* and Yi Liu

State Key Laboratory of Simulation and Regulation of Water Cycle in River Basin, *China Institute of Water Resources and Hydropower Research*, *Beijing 100038*, *P.R. China*

(*Received January 6*, *2021*, *Revised February 6*, *2025*, *Accepted February 28*, *2025*)

Abstract. Currently, the digital construction of temperature fields based on existing data (temperature field reconstruction) primarily relies on "interpolation methods" and "thermal parameter inversion methods." Although continuous advancements have been made in these approaches, the accuracy of digitally reconstructed temperature fields still requires further improvement. This paper proposes a novel methodology that establishes a finite element method-based temperature field computation framework, incorporating automated real-time corrections using measured temperature data during the calculation process, thereby achieving precise numerical reconstruction of temperature fields. Additionally, a water-cooling pipe calculation method is presented that simultaneously satisfies three critical requirements: simplified mesh discretization, accurate computation of water temperature along the flow path, and precise grid-based calculation of temperature fields surrounding cooling pipes. By employing this method, accurate temperature field reconstruction can be achieved using limited temperature measurement points without requiring thermal parameter inversion, while the inversion accuracy improves progressively with increased measurement data. This methodology lays the foundation for automated temperature field reconstruction technology based on measurement point data.

Keywords: automated; finite element method; reconstruction; temperature field

1. Introduction

Temperature cracks are the most common cracks occurring during the construction of mass concrete structures (JCI 2011, Torabi and Ansari 2018). Accurate prediction of temperature fields and calculation of thermal stresses in concrete structures are prerequisites for formulating temperature control measures to prevent cracking (ACI 207.4R 2005, Tasri and Susilawati 2019, Tia *et al*. 2010, Gajda and VanGeem 2002).

Significant advancements have been achieved in computational methods for concrete temperature field prediction. A simple and practical approach using the 3D-Finite Difference Model (3D-FDM) was developed based on MS-Excel to overcome the complexity of the other FE models (Mansour and Ebid 2023). And it was proved that concrete temperature time histories at the center and the other different locations of the bridge pile cap could be reasonably predicted using the 3D finite difference model (Mansour and Ebid 2024). By applying heat balance principles and analyzing temperature gradients around cooling pipes, Zhu *et al*. (2020) proposed a method to calculate water temperature along pipes using the buried pipe element technique. Wang *et al*. (2023a) employed ABAQUS subroutines (FILM and DFLUX) to simulate thermodynamic boundary conditions under solar radiation. Sun *et al*. (2023) proposed an equivalent method for determining hydration temperature rise rates under arbitrary thermal histories. Yang *et al*. (2025) applied MIDAS FEA NX to analyze the temperature regulation effects of phase change materials and their implications for crack resistance.

While significant progress has been made in temperature field computation, current techniques for the digital construction of temperature fields based on measured temperature data still necessitate substantial refinement. Because the composition and materials of concrete are likely to change during real-world construction processes, weather conditions at a construction site may vary, and construction methods may also be inconsistent. Thus, the temperature field predicted before construction may differ significantly from actual measurements. Therefore, accurate reconstruction of temperature fields based on real-time monitoring data is critical for effective temperature control and crack prevention in concrete structures. Currently, the following key issues require resolution:

The first method involves embedding temperature sensors or temperature-sensing optical fibers within the concrete structure and reconstructing the temperature field through interpolation of measured data. When using a small number of sensors, this approach is not practical for regions with non-linear temperature gradients. However, these regions with non-linear temperature distribution are often the focus of calculation and analysis. Consequently, reconstructing the temperature field requires dense sensor placement, leading to significant challenges, including

*Corresponding author, Ph.D., Professor,
E-mail: 1219921552@qq.com
[a] Ph.D.

ISSN: 1738-1584 (Print), 1738-1991 (Online)

construction interference, elevated costs, and operational complexity.

The second method is to use a finite element model to calculate the concrete temperature field based on the thermal parameters inverted from the measured temperature data, actual weather conditions, and construction methods. Among thermal parameters, hydration heat is influenced by the concrete temperature, and its model always contains multiple constants (De Freitas *et al*. 2013, Cervera *et al*. 2002, Bentz *et al*. 1998, Hong *et al*. 2019, Kjellsen *et al*. 1990, Tahersima *et al*. 2017). Recent advancements have demonstrated partial progress in multi-parameter inversion methodologies (Wang *et al*. 2023b, Hu *et al*. 2023, Kang *et al*. 2022, Lv *et al*. 2025). However, persistent technical limitations persist, including unresolved issues such as the algorithm's tendency to converge on local optima rather than attaining global optimal solutions during parameter inversion. Furthermore, pouring temperature discrepancies in concrete placement - particularly the impracticality of representing varied placement temperatures across distinct structural zones with fixed parameter values - have yet to be systematically investigated.

For the temperature field of mass concrete with cooling water pipes, some algorithms that model the water pipe boundary as a virtual boundary may lead to significant errors for areas near the water pipes. Additionally, algorithms that regard the water pipes as real boundaries often result in relatively low computational efficiency and complex mesh partitioning requirements due to the large temperature gradient in the concrete surrounding the pipes. Recent research advancements have demonstrated partial progress in achieving accurate temperature field computation while reducing mesh density (Li *et al*. 2024, Zhang *et al*. 2024). However, a comprehensive computational methodology for mass concrete with cooling pipes that simultaneously satisfies three critical requirements - simplified mesh discretization, precise calculation of water temperature along the flow path, and accurate grid-based thermal analysis around cooling pipes - remains technically elusive.

To solve the problems, this paper proposes a calculation method for temperature field reconstruction based on finite elements. The proposed method can be used to reconstruct a mass concrete temperature field with fewer monitoring points and does not require inversion of thermal parameters (such as surface heat release coefficient and concrete adiabatic temperature rise). The accuracy of the reconstructed temperature field rapidly approaches the true value as the number of temperature monitoring points increases. Thus, the proposed method can accurately and clearly reflect the characteristics of the concrete temperature field around a water pipe. Automated temperature reconstruction and stress calculation of concrete structures without human intervention can be also achieved by combining automatic temperature data acquisition technology with the algorithm proposed in this study (Park *et al*. 2015, Aleksandra *et al*. 2020, Kim *et al*. 2015, Azenha *et al*. 2009).

2. Finite element calculation theory for concrete temperature field

The three-dimensional heat conduction problem can be stated in an equivalent variational form as follows (Rao 2018):

Obtain the temperature distribution $T(x,y,z,t)$ inside the solid body that minimizes the integral

$$I = \frac{1}{2}\iiint_V \left[k_x \left(\frac{\partial T}{\partial x}\right)^2 + k_y \left(\frac{\partial T}{\partial y}\right)^2 + k_z \left(\frac{\partial T}{\partial z}\right)^2 - 2\left(\frac{\partial \theta}{\partial \tau} - \rho c \frac{\partial T}{\partial \underset{\sim}{t}}\right) T \right] dV \quad (1)$$

where T is the temperature; x, y and z are the coordinates in three directions respectively; v represents the solid body where it is located; k_x, k_y, and k_z are the thermal conductivity of the material in the x-direction, y-direction, and z-direction, respectively; $\frac{\partial \theta}{\partial \tau}$ is the rate of heat generated per unit volume, ρ is the density of the material, c is the specific heat of the material, and t is the time parameter.

Additionally, the following boundary conditions must be satisfied:

For the boundary condition with known temperature

$$T(x,y,z,t) = T_0 \quad (2)$$

Where t is time; T_0 is the known temperature.

For the boundary condition with known heat flow rate

$$k_x \frac{\partial T}{\partial x} l_x + k_y \frac{\partial T}{\partial y} l_y + k_z \frac{\partial T}{\partial z} l_z + q_0 = 0 \quad (3)$$

where q_0 is the boundary heat flux; l_x, l_y and l_z are the direction cosines of the outward drawn normal to the boundary.

For the boundary condition with known surface thermal convection coefficient and surrounding air (fluid) temperature

$$k_x \frac{\partial T}{\partial x} l_x + k_y \frac{\partial T}{\partial y} l_y + k_z \frac{\partial T}{\partial z} l_z + h(T - T_\infty) = 0 \quad (4)$$

where q_0 is the boundary heat flux; h is the convection heat transfer coefficient; T_∞ is the surrounding temperature.

3. New temperature field reconstruction algorithm based on finite element

For the finite element calculation values of the temperature field of a concrete structure to be consistent with the actual values, three conditions must be met: accurate concrete thermal parameters, accurate structural surface boundary conditions, and accurate water-cooling simulation. This section introduces a finite element algorithm that directly uses the temperature data of the

monitoring points, without inversion of the concrete thermal parameters (such as the adiabatic temperature rise and surface heat release coefficient), and can accurately determine the effect of water cooling.

3.1 Temperature-tracking algorithm for internal elements of concrete

This paper proposes a temperature-tracking algorithm that can accurately reconstruct the temperature field of a concrete structure based on measured data and does not require inversion of the adiabatic temperature rise and surface heat release coefficient. In addition, as the number of monitoring points increases and the calculation time step shortens, the reconstructed temperatures will approach the true values. During the time-domain discretization and step-by-step calculation process, the calculated value is always adjusted and approaches the true value; thus, this algorithm is referred to as the temperature-tracking algorithm.

3.1.1 Temperature-tracking algorithm for internal elements of concrete

To accurately calculate the convection coefficient of concrete surface and avoid repeated inversion of internal temperature of concrete, an algorithm was invented by authors of this paper to track the internal temperature of concrete and obtained the authorization of Chinese patent (Liu *et al*. 2020). This method is described in detail below:

The elements containing the concrete surface nodes and the elements sharing the same nodes are defined as the surface structural elements, and the remaining elements are defined as the internal structural elements.

In this study, the adiabatic temperature-rise parameter in the heat-transfer equation for concrete was modified. The modified adiabatic temperature-rise parameter no longer represents the hydration heat release performance of concrete, but its expression and finite element discretization method are consistent with Eq. (1). In this study, this modified adiabatic temperature-rise parameter is defined as the concrete temperature-change parameter, the solution method for which is described as follows.

For any point b on a concrete structure, if the point is a monitoring point, then the measured temperature is the temperature of the monitoring point. Otherwise, if point b is not a monitoring point and there are m monitoring points with temperatures T_{cn1}, T_{cn2}, ⋯, T_{cnm} on the corresponding pouring layer (as shown in Fig. 1), and the distances between the monitoring points and point b are d_1, d_2, d_3⋯, d_m then the measured temperature T_{bcn} of point b can be fitted using

$$T_{bcn} = \sum_{i=1}^{m} \frac{T_{cni} d_i^e}{D} \tag{5}$$

In Eq. (5), $D = \sum_1^m d_i^e$, i denotes the serial number of each monitoring point, m is the number of monitoring points, T_{cni} is the temperature of the i_{th} monitoring point at the n_{th} calculation step, d_{i} is the distance from the monitoring point to point b, T_{bcn} is the measured temperature of point b calculated at the n_{th} step, and e is a constant.

As shown in Fig. 2, when calculating the temperature of a concrete structure using the finite element method, if point b is on the centroid of an internal concrete element, the time-discrete format of the temperature-change parameter can be expressed as

$$\frac{\partial \theta}{\partial \tau} = \frac{T_{bcn} - T_{bn-1}}{t_n - t_{n-1}} \tag{6}$$

where T_{bcn} is the measured temperature of point b calculated at the n_{th} step, and $T_{bn\text{-}1}$ is the calculated temperature of point b at the $(n\text{ -}1)_{\text{ th}}$ step.

If the boundary conditions are real in the calculation steps of each time period, the temperature-change parameter is the adiabatic temperature rise. If the boundary conditions are different from the real boundary conditions and $T_{bn\text{-}1}$ is lower than the actual value, the temperature-change parameter at the n_{th} step will be greater than the adiabatic temperature rise and will offset the boundary condition errors. Therefore, the calculation result will be close to the actual solution. Similarly, if the boundary conditions are different from the real boundary conditions and $T_{bn\text{-}1}$ is higher than the actual value, the temperature-change parameter will be less than the actual adiabatic temperature rise and will offset the boundary condition errors; thus, the calculation result approach the actual value. The influence of the external environment on the concrete interior exhibits hysteretic characteristics. After replacing the adiabatic temperature-rise parameter with the temperature-change parameter for the finite element calculation, even if there is a large deviation from the actual boundary conditions, the temperature of the internal element of the concrete can still approach the true value if the time step is shortened.

Therefore, if Eq. (6) is used to calculate the temperature field—regardless of whether the concrete material properties, boundary conditions, and other factors are accurate, the concrete temperature field near the monitoring

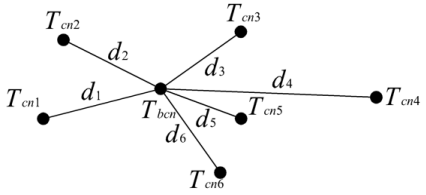

Fig. 1 Relationship between internal monitoring points and an arbitrary point b in a concrete structure

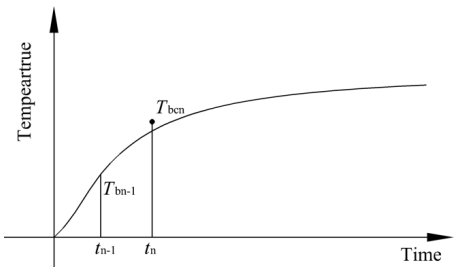

Fig. 2 Relationship between monitoring data and calculation data of a concrete structure

point will be accurate as long as the time step is sufficiently short. If the effect of the temperature history on the concrete hydration heat release can be neglected and the boundary conditions of the structure can be accurately simulated, the temperature field of the concrete structure can be accurately reconstructed by arranging only one temperature monitoring point in each pouring layer. However, to account for inconsistencies in the pouring temperature and material properties, the inaccurate boundary conditions, and the effect of the temperature history on concrete hydration, it is necessary to arrange several temperature monitoring points in the internal concrete elements.

Concrete is a poor conductor of heat, and the local temperature distribution of concrete structures may be highly non-linear. Therefore, if Eq. (5) and the temperature of the monitoring point are used directly to fit the temperatures of regions without monitoring points, the calculation accuracy will generally be very poor. However, like the adiabatic temperature rise of concrete, the temperature-change parameter inside a structure does not have a highly non-linear distribution in a specific time calculation step. It is even considered as constant in ordinary temperature-field calculations. Fitting the temperature-change parameter using the difference method can deliver a high accuracy with only a small number of temperature monitoring points. The essence of Eq. (6) is to use the method of difference to determine the temperature-change parameter of the internal element. Therefore, based on Eq. (6) and the finite element method, if the boundary conditions are accurate, the temperature field of concrete structures can be reconstructed accurately by arranging only a small number of monitoring points inside the pouring layers.

The error of this method only depends on the time span of the calculation step. Theoretically, the temperature of the monitoring point can be infinitely close to the true value as the time step was shortened.

3.1.2 Temperature-tracking algorithm for surface elements

The surface elements of concrete can be considered the equivalent of the surface boundary conditions for a concrete structure; that is, if the temperatures of all the nodes on a concrete surface element are accurate, then the surface boundary conditions of the concrete structure can be considered accurate. Concrete is a poor conductor of heat, and the heat release performance of concrete surface elements may differ substantially from that of internal elements. Although the tracking algorithm can be used for calculation, it needs to consider the surface elements separately from the internal elements. Generally, when no temperature monitoring points are arranged inside a surface element, the boundary conditions of mass concrete will be the first or second type of boundary condition expressed Eqs. (2) and (3), respectively, and the calculation accuracy will depend on the detail and precision of the boundary conditions. However, if a thermometer is placed very close to a concrete surface (e.g. 5 cm), then, using the temperature-tracking algorithm for the surface elements of the concrete structure, the node temperatures will approach the true value with reductions in the calculation step size. This will occur even when the calculated boundary conditions are very different from the actual boundary conditions.

As different insulation materials can be applied on a concrete surface and because a concrete structure can block solar radiation, the boundary conditions of different areas of a concrete surface may vary significantly. Thus, it is necessary to divide the surface of a structure into several areas according to factors such as the application of insulation materials, and to analyze each area separately.

First, an area with the same boundary conditions is selected. For any point on a selected concrete surface element, if the point is a monitoring point, the measured temperature of the point is the temperature of the monitoring point. If point b is an internal point on a surface element and there are k monitoring points on the surface elements that are in the same pouring layer as point b, the temperatures of the monitoring points are T_{cn1}, T_{cn2}, $\cdots$, T_{cnk}, and the distances between the monitoring points and point b are d_1, d_2, $d_3\cdots$, d_k. Then, the measured temperature T_{bcn} of point b can be fitted as

$$T_{bcn} = \sum_{i=1}^{k} \frac{T_{cni} d_i^e}{D} \tag{7}$$

In Eq. (7), $D = \sum_1^k d_i^e$, i denotes the serial number of each monitoring point, m is the number of monitoring points, T_{cni} is the temperature of the i_{th} monitoring point at the n_{th} calculation step, d_i is the distance from the monitoring point to point b, T_{bcn} is the measured temperature of point b calculated at the nth step, and e is a constant.

The calculation method for the temperature-change parameter for surface elements is the same as Eq. (6). Although the value of the surface heat release coefficient will not affect the calculation accuracy of the reconstructed temperature field, it may significantly affect the calculation efficiency. This is because if there is a large difference between the calculated surface heat release coefficient and the actual coefficient, a very short time step will be required. Therefore, it is necessary to select a reasonable surface heat release coefficient to ensure efficient calculation.

This method requires thermometers to be embedded inside the surface element. It is recommended to embed at least one thermometer in areas with different solar radiation shielding and surface insulation conditions. Because adding thermometers will not significantly increase the cost of reconstructing the temperature field, it is recommended to place more thermometers on the surface area. However, if the accuracy of the reconstructed temperature field can be sacrificed, the estimated surface heat release coefficient can be used to perform simulation analysis for the non-key study areas, and the temperature-tracking algorithm can be used to reconstruct the temperature field for the key study areas.

3.2 Treatment of boundary conditions for water pipes based on heat-flow balance

3.2.1 Temperature calculation method for mass concrete containing water pipes

Because concrete is a poor conductor of heat, the concrete temperature gradient around a water pipe is relatively large. Moreover, the temperature monitoring point itself has a certain thickness, and the thermal conductivity of its protective material is usually very low. Therefore, it is challenging to measure the temperature around a water pipe accurately using ordinary thermometers. Because the premise for ensuring accuracy for the proposed tracking algorithm is that the measured values of the temperature monitoring points are accurate, the tracking algorithm may not accurately reflect the temperature of concrete around a water pipe.

Several methods are available for calculating the temperature field of mass concrete containing water pipes. For example, if the calculation amount allows, the most direct method is to arrange a series of nodes along the direction of the water pipe and assign accurate temperatures at these nodes. However, the following two problems must be solved before using this method:

(1) Generally, the only water temperatures that can be monitored during concrete pouring are the inlet and the outlet water temperatures. However, the distribution of water temperature inside a water pipe is highly non-linear. Thus, the challenge is accurately calculating the water temperature distribution along the water pipe.

(2) At present, plastic water pipes are widely used in temperature-controlled mass concrete cooling. Because of the low thermal conductivity of plastic water pipes, the water temperature in the pipe is not equal to the node temperature. Thus, the challenge is calculating the relationship between the water temperature in the water pipe and the node temperature.

The aforementioned factors limit the reconstruction accuracy of the concrete temperature field around a water pipe. This study provides a method that can accurately consider the temperature of a node where a water pipe is located, thereby improving the temperature field reconstruction accuracy for mass concrete containing water pipes.

3.2.2 Temperature field distribution of concrete around a water pipe

At present, there are many algorithms for temperature field of mass concrete with cooling pipes (Myers *et al.* 2009, Singh and Rai 2018). This paper presents a high-precision calculation method for small element size, which is suitable for reconstruction of temperature field.

Fig. 3 shows a typical cross-section of water pipe-containing mass concrete in the direction vertical to the water pipe. The red circle in the figure represents the cooling water pipe, the inner and outer radii of which are r_i and r_o, respectively. As shown in Fig. 3, the concrete around the water pipe is defined as area A (i.e., the area with inner and outer radii of r_o and r_d in Fig. 3), and the concrete outside area A is defined as area B. The temperature gradient of area A can be expressed as a function of four physical quantities, namely the heat flow from area B to area A, the change in the hydration heat release of area A over time, the change in the heat of area A over time, and the water temperature.

Both the changes in the hydration heat release and in the heat of area A are closely related to the volume of the concrete. If the volume of area A is sufficiently small, these changes can be ignored. Author et al. highlighted that if the outer radius of area A is less than 0.10 m, it can be assumed that the temperature of area A is only related to the heat flow and the temperature of the water transferred from area B to area A (Zhu *et al.* 2013). Then, the temperature gradient in the water pipe and that in the concrete in area A can be expressed as

$$G(r_x)=\begin{cases} k\dfrac{r_0}{r_x} & r_i \le r_x \le r_o \\ \dfrac{k\lambda_p r_0}{\lambda_c r_x} & r_o \le r_x \le r_d \end{cases} \tag{8}$$

where r_i is the inner radius of the water pipe, r_o is the outer radius of the water pipe, λ_p is the thermal conductivity of the water pipe material, λ_c is the thermal conductivity of concrete, and k is the water pipe-side temperature gradient at the interface between the water pipe and the concrete.

The temperature difference between the inner and outer walls of the water pipe can be obtained by integrating Eq. (8)

$$\Delta T_{oi} = k r_o \ln\left(\frac{r_o}{r_i}\right) \tag{9}$$

Similarly, the temperature difference between a location r_d from the water pipe and the outer wall of the water pipe (i.e., the interface between the water pipe and the concrete) can also be obtained by integrating Eq. (8)

$$\Delta T_{oi} = k r_o \frac{\lambda_p}{\lambda_c} ln\left(\frac{r_d}{r_o}\right) \tag{10}$$

From Eqs. (9) and (10), the temperature gradient at the inner wall of the water pipe (i.e., the interface between the water pipe and the water) can be obtained as follows

$$G(r_i)=\frac{T_d - T_w}{\left[\ln\left(\frac{r_o}{r_i}\right)+\frac{\lambda_p}{\lambda_c}\ln\left(\frac{r_d}{r_o}\right)\right] r_i} \tag{11}$$

where T_w is the water temperature, and T_d is the temperature

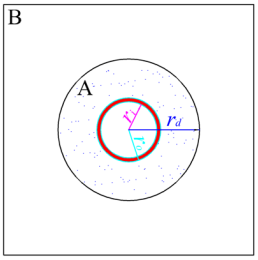

Fig. 3 Typical cross-section of a cooling water pipe in mass concrete

of the location at a distance d from the water pipe.

Similarly, according to Eqs. (9) and (10), the temperature of the outer wall of the water pipe (i.e., the interface between the water pipe and the concrete) can be expressed as

$$T_p = T_w + \frac{\ln\left(\frac{r_o}{r_i}\right)}{\ln\left(\frac{r_o}{r_i}\right) + \frac{\lambda_p}{\lambda_c}\ln\left(\frac{r_d}{r_o}\right)}(T_d - T_w) \tag{12}$$

3.2.3 Calculation of water temperature along a water pipe

According to the literature, the increment in water temperature along a water pipe of length *dl* can be expressed as

$$\Delta T_{\mathrm{wi}} = \frac{-\lambda_p}{c_w \rho_w q_w} \iint_{\Gamma 0} \frac{\partial T}{\partial n} ds \tag{13}$$

where c_w is the specific heat of water, ρ_w is the density of water, q_w is the heat flow, dl is a micro element of the water pipe section, $\partial T/\partial n$ is the temperature gradient, and λ_p is the thermal conductivity of the water pipe material.

The temperature gradient around a water pipe is regarded as constant. According to Eq. (11)

$$\frac{\partial T}{\partial n} = \frac{T_{w_i} - T_d}{\left[\ln\left(\frac{r_o}{r_i}\right) + \frac{\lambda_p}{\lambda_c}\ln\left(\frac{r_d}{r_o}\right)\right] r_i} \tag{14}$$

Evidently, $\iint_{\Gamma 0} ds = 2\pi r_i dl$, and

$$\Delta T_{\mathrm{wi}} = \frac{2\pi dl \lambda_p (T_d - T_{wi})}{c_w \rho_w q_w \left[\ln\left(\frac{r_o}{r_i}\right) + \frac{\lambda_p}{\lambda_c}\ln\left(\frac{r_d}{r_o}\right)\right]} \tag{15}$$

As the inlet temperature of the cooling water is known, Eq. (15) can be used to calculate the water temperature of each cooling water pipe along the direction of the water flow. Let a certain cooling water pipe be divided into *m* sections, the inlet water temperature be T_{w0}, and the increment in water temperature in the i_{th} water pipe section be ΔT_{wi}. Then

$$T_{\mathrm{wi}} = T_{w0} + \sum_{j=1}^{i} \Delta T_{\mathrm{wj}}, \quad i = 1,2,3,\cdots,m \tag{16}$$

Because both Eqs. (15) and (26) contain the water temperature variable and are not explicit equations, the temperature field cannot be obtained in one step. An iterative solution method must be used to obtain the actual solution gradually. In the first iteration, it can be assumed that the water temperature along the entire cooling water pipe is equal to the inlet temperature of the cooling water, and the approximate temperature field can be obtained using Eq. (1). Subsequently, Eqs. (15) and (16) can be used to obtain the water temperature along the water pipe. The iterations are repeated until a stable solution is obtained.

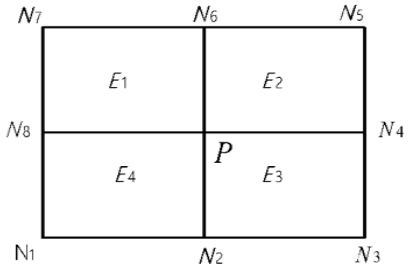

Fig. 4 Element where water pipe node is located

2.2.4 Solving the finite element node temperature

For the finite element mesh, the node diagram in Fig. 4 is used as an example. *P* is a node on the water pipe, and N_1, N_2, ⋯, N_j, ⋯, N_m are the m nodes that are not on the water pipe and share common elements with node *P*.

Let the distance between node N_i and node *P* be r_{di}. Then, the m temperatures of node *P* and the temperature along the water pipe of length *dl*, denoted as T_{pj} and ΔT_{wj}, respectively, can be obtained using Eqs. (12) and (15), respectively.

Then, the temperature of node *P* can be expressed as

$$T_p = \frac{\sum_{j=1}^{m} T_{pi}}{m} \tag{17}$$

The temperature increment along the water pipe of length *dl* can be expressed as

$$\Delta T_{\mathrm{wi}} = \frac{\sum_{j=1}^{m} \Delta T_{\mathrm{wij}}}{m} \tag{18}$$

If the size of the element where node *P* is located meets the requirements of Eq. (8), then Eqs. (16)-(18) will yield the temperatures of the nodes where the water pipe is located. By applying the first type of boundary condition, given in Eq. (2), the boundary condition of the water pipe can be simulated accurately.

4. Calculation example

4.1 Test introduction

A concrete test block was used to verify the accuracy of the proposed algorithm. The known thermal properties of the concrete were its thermal conductivity and temperature conductivity. Within 6.5 d of pouring, 5 cm of polyurethane was sprayed on the outer side of the steel formwork on the four sides of the concrete. After 6.5 d of pouring, 10 cm of benzene boards were placed on the S-1 and S-3 sides, and 5 cm and 10 cm of polyurethane were sprayed on the S-2 and S-4 sides, respectively. The properties of all insulation materials were unknown.

As shown in Fig. 5(a), the test block used in this study had dimensions of 5 m × 5 m × 3 m, and thermometers were placed on the EFGH and ABCD sections as shown in Fig. 5(a).

Plastic cooling water pipes with an inner diameter of 28 mm and an outer diameter of 32 mm were installed 1.5 m away from the concrete. The layout of the cooling water pipes is shown in Fig. 5(d). After the concrete was poured, the water cooling was started. The inlet water temperature

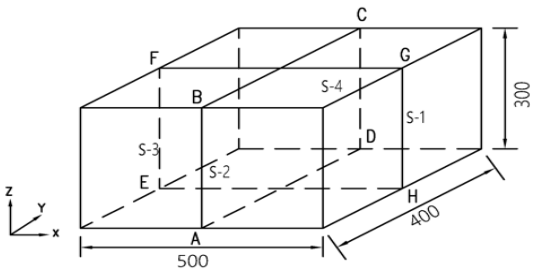

(a) Test block dimensions

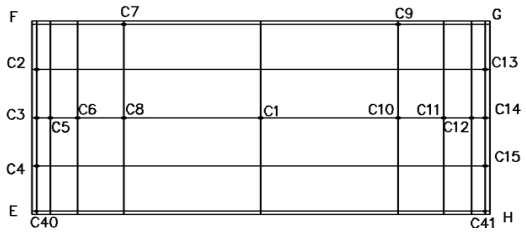

(b) Thermometer layout on section EFGH

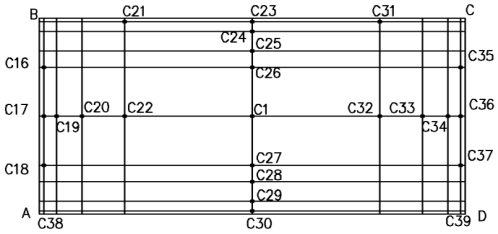

(c) Thermometer layout on section ABCD

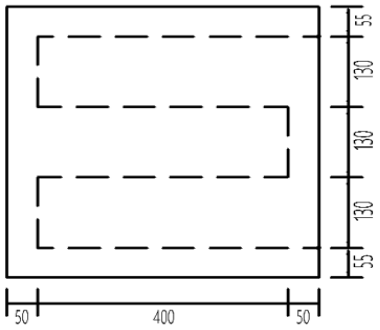

(d) Layout of cooling water pipes

Fig. 5 Dimensions of pouring block and locations of thermometers

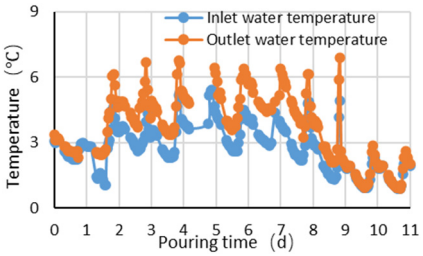

(a) Inlet and outlet water temperatures

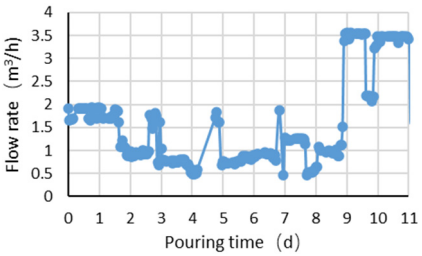

(b) Flow rate

Fig. 6 Measured inlet and outlet water temperatures and flow rate

(a) Layout of monitoring points and water pipes

(b) Construction process

(c) Spraying of insulation materials before demolding

(d) Insulation materials after demolding

Fig. 7 Concrete monitoring point layout, pouring, and insulation

and flow rate are shown in Fig. 6.

On-site images of the layout of the concrete monitoring points, the pouring, the spraying of polyurethane on the outer side of the steel formwork, and the thermal insulation material cover after demolding are shown in Fig. 7.

4.2 Temperature-field reconstruction results

Based on actual measurements of the temperature field of the test block, the proposed algorithm was used to reconstruct the temperature field of the test block. The finite element time step in the reconstruction process was set as 0.025 d. As shown in Fig. 5, in the inversion process, monitoring points C30, C38, C39, C40, and C41 tracked the temperature of the bottom surface. C23 tracked the temperature of the top surface. C13, C14, and C15 tracked the temperature of the S-1 surface. C16, C17, and C18 tracked the temperature of the S-2 surface. C2, C3, and C4 tracked the temperature of the S-3 surface, and C35, C36, and C37 tracked the temperature of the S-4 surface.

According to the results of the previous analysis, the temperature data from the monitoring points on the water pipe wall cannot represent the actual temperature data. The monitoring points that track the internal temperature of concrete do not include those near the wall of a water pipe. Eighteen days before pouring, all the internal temperature monitoring points except those on the water pipe wall were used for the tracking calculation; 18 d after pouring, only C1, C26, and C27 were used in the tracking calculation.

The temperature distributions of the surface, cross-section A, and cross-section B in the reconstructed temperature field of the concrete on the 2nd, 10th, and 28th days after pouring are shown in Figs. 8, 9, and 10, respectively. The reconstructed temperature field completely conformed to the general temperature field distribution pattern. The errors between the measured values that were used in the tracking calculation and the corresponding true values can be controlled by shortening the finite element time step. For brevity, only monitoring points C1–C6 are discussed. As shown in Fig. 11, when the time step was 0.025 d, the errors between the measured values and the calculated values were all within 0.2°C.

(a) Surface temperature distribution (b) Cross-section temperature distribution

Fig. 8 Surface and cross-section temperature distributions on 2nd day after pouring

(a) Surface temperature distribution (b) Cross-section temperature distribution

Fig. 9 Surface and cross-section temperature distributions on 10th day after pouring

(a) Surface temperature distribution (b) Cross-section temperature distribution

Fig. 10 Surface and cross-section temperature distributions on 28th day after pouring

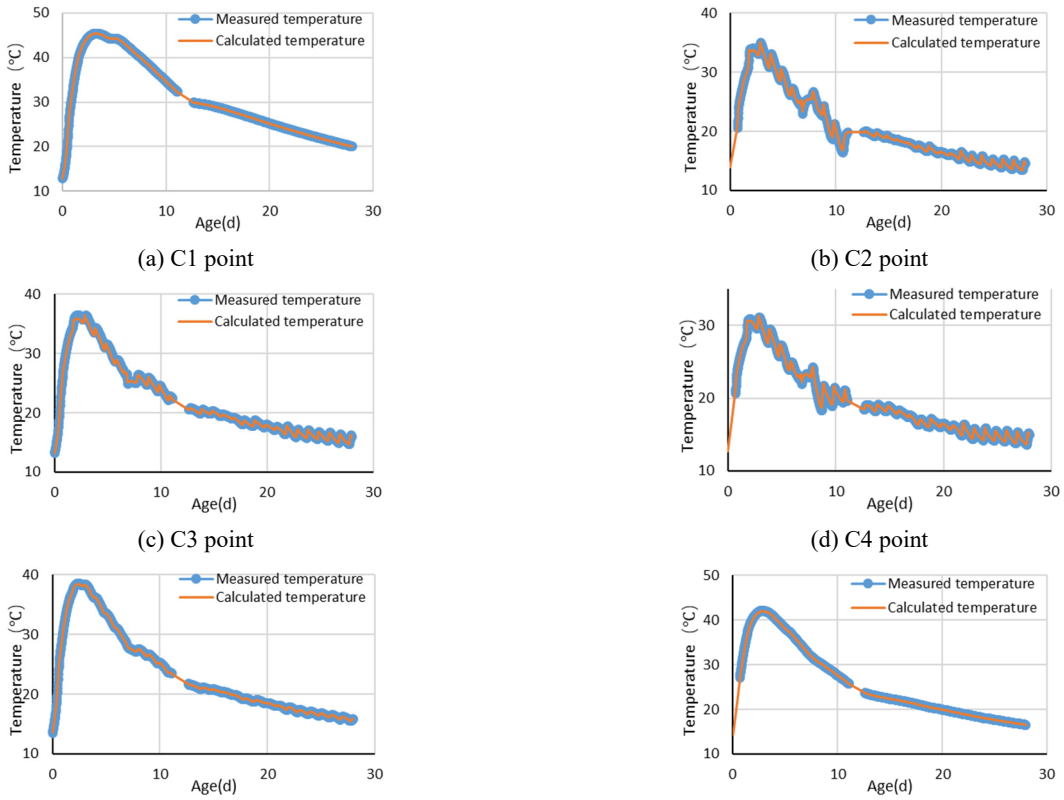

(a) C1 point (b) C2 point

(c) C3 point (d) C4 point

(e) C5 point (f) C6 point

Fig. 11 Measured and calculated temperatures of monitoring points

Eighteen days after pouring, when only three monitoring points were used in the tracking calculation, using monitoring points 5 and 6 as examples—it can be seen that the calculated temperature process line almost coincided with the measured line. These results indicate that a high accuracy can be achieved by arranging only a small number of monitoring points inside the pouring block when using the proposed algorithm.

5. Conclusions

In this study, a temperature-tracking algorithm was developed to reconstruct the temperature field of concrete, and the heat flow balance method was adopted to calculate the temperatures of nodes at water pipes in mass concrete. The proposed method can be used to reconstruct the temperature field without inversion of the surface heat release coefficient and concrete adiabatic temperature rise. Moreover, the calculation examples provided herein showed that in the temperature field reconstructed using the proposed algorithm, the temperature of the monitoring point can be infinitely close to the true value as the time step was shortened. Furthermore, only a small number of monitoring points are needed for accurately reconstructing the temperature field of mass concrete containing water pipes. In addition, automatic reconstruction and calculation of the temperature and stress of concrete structures without human intervention can be realized using the proposed algorithm.

This study proposes an explicit temperature field reconstruction algorithm for temperature field that requires smaller computational time steps. The time step of the proposed algorithm needs to be very short for accurate reconstruction of a temperature field when there are large deviations between the calculated boundary conditions and the actual boundary conditions. With this study, the calculation efficiency of the proposed algorithm is only suitable for temperature field reconstruction of slices, aqueducts, and other small-scale mass concrete structures. Thus, this necessitates concurrent research into maintaining computational accuracy while implementing enlarged time steps.

Acknowledgments

The research described in this paper was financially supported by the National Key R&D Program of China (Grant no. 2018YFC0406703), the National Natural Science Foundation of China (Grant no. 51779277,51779276), Special Research Project of China Institute of Water Resources & Hydropower Research (Grant no. SS0145B612017, SS0145B392016), Self-Topic Fund of State Key Laboratory of Simulation & Regulation of Water Cycle in River Basin (Grant no. SKL2020ZY10).

References

ACI 207.4R (2005), Cooling and Insulating Systems for Mass Concrete; American Concrete Institute, Farmington Hills, MI, USA.

Aleksandra, K.C., Krzysztof, W. and Jacek, C. (2020), "Prediction of cast-in-place concrete strength of the extradosed bridge deck based on temperature monitoring and numerical simulations", *Constr. Build. Mater.*, **254**, 119224. https://doi.org/10.1016/j.conbuildmat.2020.119224

Azenha, M., Faria, R. and Ferreira, D. (2009), "Dentification of early-age concrete temperatures and strains: Monitoring and numerical simulation", *Cement Concrete Compos.*, **31**(6), 369-378. https://doi.org/10.1016/j.cemconcomp.2009.03.004

Bentz, D.P., Waller, V. and de Larrard, F. (1998), "Prediction of adiabatic temperature rise in conventional and high-performance concretes using a 3-D microstructural model", *Cem. Concrete Res.*, **28**, 285-297. https://doi.org/10.1016/S0008-8846(97)00264-0

Cervera, M., Faria, R., Oliver, J. and Prato, T. (2002), "Numerical modelling of concrete curing, regarding hydration and temperature phenomena", *Comput. Struct.*, **80**, 1511-1521. https://doi.org/10.1016/S0045-7949(02)00104-9

De Freitas, J.T., Cuong, P.T., Faria, R. and Azenha, M. (2013), "Modelling of cement hydration in concrete structures with hybrid finite elements", *Finite Elem. Anal. Des.*, **77**, 16-30. https://doi.org/10.1016/j.finel.2013.07.008

Gajda, J. and Vangeem, M. (2002), "Controlling temperatures in mass concrete", In: *Concrete International*, American Concrete Institute, Farmington Hills, MI, USA, **24**(1), pp. 58-62.

Hong, Y., Lin, J. and Chen, W. (2019), "Simulation of thermal field in mass concrete structures with cooling pipes by the localized radial basis function collocation method", *Int. J. Heat Mass Tran.*, **129**, 449-459. https://doi.org/10.1016/j.ijheatmasstransfer.2018.09.037

Hu, Y., Bao, T., Ge, P., Tang, F., Zhu, Z. and Gong, J. (2023), "Intelligent inversion analysis of thermal parameters for distributed monitoring data", *J. Build. Eng.*, **68**, 106200. https://doi.org/10.1016/j.jobe.2023.106200

JCI (2011), JCI Guidelines for Control of Cracking of Mass Concrete 2008; Japan Concrete Institute, Tokyo, Japan.

Kang, F., Liu, X., Li, J. and Li, H. (2022), "Multi-parameter inverse analysis of concrete dams using kernel extreme learning machines-based response surface model", *Eng. Struct.*, **256**, 113999. https://doi.org/10.1016/j.engstruct.2022.113999

Kim, J., Luis, R., Smith, M.S., Figueroa, J.A., Malocha, D.C. and Nam, B.H. (2015), "Concrete temperature monitoring using passive wireless surface acoustic wave sensor system", *Sensor Actuat. A-Phys.*, **224**, 131-139. https://doi.org/10.1016/j.sna.2015.01.028

Kjellsen, K.O., Detwiler, R.J. and Gjørv, O.E. (1990), "Pore structure of plain cement pastes hydrated at different temperatures", *Cem. Concrete Res.*, **20**, 927-933. https://doi.org/10.1016/0008-8846(90)90055-3

Li, Q., Chen, G. and Zhu, F. (2024), "Simulation of thermal field in mass concrete with cooling pipes based on the isogeometric analysis method", *Front. Phys.*, **12**, p. 1338718. https://doi.org/10.3389/fphy.2024.1338718

Lv, Z., Ding, Y. and Zhang, Y. (2025), "Study on Long-Term Temperature Variation Characteristics of Concrete Bridge Tower Cracks Based on Deep Learning", *Sensors*, **25**(1), 207. https://doi.org/10.3390/s25010207

Liu, Y., Zhu, Z., Zhang, G., Yang, N., Wu, C., Fang, Z., Liu, Y., Wang, Z., Zhang, L., Yang, P., Li, H., Yang, Z., Mou, R., Chen, W. and Tan, Y. (2020), "Real time back analysis method for surface heat release coefficient of concrete dam block", CN201910353812.7.

Mansour, D.M. and Ebid, A.M. (2023), "Modeling of heat transfer in massive concrete foundations using 3D-FDM", *Civil Eng. J.-Tehran*, **9**(10), 2430-2444. http://dx.doi.org/10.28991/CEJ-2023-09-10-05

Mansour, D.M. and Ebid, A.M. (2024), "Predicting thermal behavior of mass concrete elements using 3D finite difference model", *Asian J. Civil Eng.*, **25**, 1601-1611. https://doi.org/10.1007/s42107-023-00864-2

Myers, T.G., Fowkes, N.D. and Ballim, Y. (2009), "Modeling the cooling of concrete by piped water", *J. Eng. Mech.*, **135**(12), 1375-1383. https://doi.org/10.1061/(ASCE)EM.1943-7889.000004

Park, J.H., Huynh, T.C. and Kim, J.T. (2015), "Temperature effect on wireless impedance monitoring in tendon anchorage of prestressed concrete girder", *Smart Struct. Syst., Int. J.*, **15**(4), 1159-1175. https://doi.org/10.12989/sss.2015.15.4.1159

Rao, S.S. (2018), *The Finite Element Method in Engineering*, Butterworth-Heinemann.

Singh, P.R. and Rai, D.C. (2018), "Effect of piped water cooling on thermal stress in mass concrete at early ages", *J. Eng. Mech.*, **144**(3), p. 04017183. https://doi.org/10.1061/(ASCE)EM.1943-7889.0001418

Sun, Q., Zhang, B., Shi, K., Gupta, R., Zhu, Z. and Qiang, S. (2023), "A novel method for solving hydration heat release based on equivalent heat release theory", *Constr. Build. Mater.*, **407**, p. 133506. https://doi.org/10.1016/j.conbuildmat.2023.133506

Tahersima, M., Ley, T. and Tikalsky, P. (2017), "Hydration Heat in a mass concrete and a thin slab with limestone blended cement", *Int. J. Mater. Sci. Eng.*, **5**(2), 79-86. https://doi.org/10.17706/ijmse.2017.5.2.79-86

Tasri, A. and Susilawati, A. (2019), "Effect of cooling water temperature and space between cooling pipes of post-cooling system on temperature and thermal stress in mass concrete", *J. Build. Eng.*, **24**, 100731. https://doi.org/10.1016/j.jobe.2019.100731

Tia, M., Ferraro, C.C., Lawrence, A., Smith, S. and Ochiai, F. (2010), Development of design parameters for mass concrete using finite element analysis; Florida Department of Transportation, Gainesville, FL, USA.

Torabi, J. and Ansari, R. (2018), "Thermally induced mechanical analysis of temperature dependent FG-CNTRC conical shells", *Struct. Eng. Mech., Int. J.*, **68**(3), 313-323. https://doi.org/10.12989/sem.2018.68.3.313

Wang, Q., Xian, J., Xiao, J. and Zou, S. (2023a), "Simulation study on sunshine temperature field of a concrete box girder of the cable-stayed bridge", *Sustainability*, **15**, p. 7541. https://doi.org/10.3390/su15097541

Wang, F., Zhao, C., Zhou, Y., Zhou, H., Liang, Z., Wang, F., Seman, E.A. and Zheng, A. (2023b), "Multiple thermal parameter inversion for concrete dams using an integrated surrogate model", *Appl. Sci.*, **13**, p. 5407. https://doi.org/10.3390/app13095407

Yang, K., Zhang, W., Chen, R., Duan, M. and Shangguan, H. (2025), "Simulation Analysis of Temperature Field and Stress Field of Mass Concrete Under Different Construction Temperatures", *Buildings*, **15**(3), p. 370. https://doi.org/10.3390/buildings15030370

Zhang, H., Su, C., Song, Z., Shen, Z. and Lei, H. (2024), "Calculation of Mass Concrete Temperature Containing Cooling Water Pipe Based on Substructure and Iteration Algorithm", *CMES-Compos. Modell. Eng. Sci.*, **138**(1), 813-826. https://doi.org/10.32604/cmes.2023.030055

Zhu, Z., Qiang, S. and Chen, W. (2013), "A new method solving the temperature field of concrete around cooling pipes", *Comput. Concrete, Int. J.*, **11**(5), 441-462. https://doi.org/10.12989/cac.2013.11.5.441

Zhu, Z., Liu, Y., Fan, Z., Qiang, S., Xie, Z., Chen, W. and Wu, C. (2020), "Improved buried pipe element method for temperature-field calculation of mass concrete with cooling pipes", *Eng. Computat.*, **37**(8), 2619-2640. https://doi.org/10.1108/EC-09-2019-0439